

Ballistic resistivity in aluminum nanocontacts

A. Hasmy¹, A.J. Pérez-Jiménez², J.J. Palacios², P. García-Mochales³,
J.L. Costa-Krämer⁴, M. Díaz¹, E. Medina¹, and P.A. Serena³

¹*Centro de Física, IVIC, Apdo. 21827, Caracas 1020A, Venezuela*

²*Departamento de Física Aplicada, Universidad de Alicante,
San Vicente del Raspeig, 03690-Alicante, Spain*

³*Instituto de Ciencia de Materiales de Madrid, CSIC, Cantoblanco, 28049-Madrid, Spain*

⁴*Instituto de Microelectrónica de Madrid, CSIC, Isaac Newton 8, PTM,
28760-Tres Cantos, Madrid, Spain*

Abstract

One of the major industrial challenges is to profit from some fascinating physical features present at the nanoscale. The production of dissipationless nanoswitches (or nanocontacts) is one of such attractive applications. Nevertheless, the lack of knowledge of the real efficiency of electronic ballistic/non dissipative transport limits future innovations. For multi-valent metallic nanosystems -where several transport channels per atom are involved- the only experimental technique available for statistical transport characterization is the conductance histogram. Unfortunately its interpretation is difficult because transport and mechanical properties are intrinsically interlaced. We perform a representative series of semiclassical molecular dynamics simulations of aluminum nanocontact breakages, coupled to full quantum conductance calculations, and put in evidence a linear relationship between the conductance and the contact minimum cross-section for the geometrically favored aluminum nanocontact configurations. Valid in a broad range of conductance values, such relation allows the definition of a transport parameter for nanomaterials, that represents the novel concept of ballistic resistivity.

If the mean free path of electrons is larger than the nanocontact size, the transport supported by propagating channels is expected to be ballistic (i.e., for aluminum, at room temperature, the electron mean free path is 45 nm, whereas at 4K it is of the order of millimeter). For contact sizes of the order of a few Fermi wavelengths λ_F , well defined modes (channels) appear associated to the transversal confinement of electrons. In such limit, the conductance G is well described by the Landauer formula $G = G_0 \sum_{n=1}^N T_n$, where $G_0 = 2e^2/h$ is the conductance quantum (e being the electron charge and h Planck's constant), T_n is the transmission probability of the n -th channel, and N is the number of propagating modes with energies below the Fermi energy [1]. Previous studies [2] demonstrated that, in principle, the number of conducting channels are determined by the number of valence electrons of the respective chemical element, and the transport efficiency or transmission probability of electrons can differ significantly depending on the nanocontact structure [3]. While for monovalent noble-metals such as Cu, Ag and Au, the transmission probability T has been estimated to be approximately equal to 1 (i.e. at a nanocontact neck, each noble metal atom contributes with G_0 to the conductance value [4,5]), for some monovalent alkali-metals or polyvalent chemical species, the channel transmittivity can result smaller than one in single-atom contacts [2,5,6]. The few detailed studies available in the literature relate to single-atom contacts [2]. It has been evidenced that the only electronic channel available to a single-atom gold contact has a better transmission performance than any single electronic channel, of the possible three, for the aluminum atom [2,4]. Thus, more channels do not guarantee better transport at the atomic scale. The transmission efficiency has its origin in the scattering processes taking place associated with the particular electronic structure of the atoms forming the nanocontact region. Then, existing ballistic theories that relate the conductance with the contact size (namely, the Sharvin formula [7] with its semiclassical corrections within the free electron model [8]), fail because they neglect the 'chemistry' in nanoconstrictions.

Electronic transport measurements on metallic nanocontacts of different sizes, have been made possible by means of scanning tunnelling microscopy (STM) [9], mechanically con-

trollable break-junctions (MCBJ) [10,11], or simply separating two macroscopic wires in table-top experiments [12]. By indenting one electrode into another and then separating them, one observes a stepwise decrease in the electrical conductance, until the breakpoint is reached, corresponding to the formation of a single-atom nanocontact. Each scan of the conductance dependence on elongation differ from one another, since structural evolutions during breakages are not identical [13]. However, statistically, the accumulation of data from many scans gives rise to a histogram of peaked structures, a clear evidence for the existence of preferential conductance values. Such conductance histograms are a robust reproducible characteristic for a given metal species under fixed experimental parameters (such as temperature and applied voltage). On the other hand, recent molecular dynamics simulations of a series of aluminum nanocontact breakages, reveal a peaked structure corresponding to preferred geometrical configurations at the nanocontact neck [13]. In spite of the quantum features of conductance at the atomic scale, these results suggest that a relation exists between preferred atomic configurations and the conductance histogram peaks [14–16].

We have implemented a state-of-the-art Embedded Atom Molecular Dynamics method for the simulations of aluminum nanocontact rupture [13,14,17]. The atoms were initially distributed in a supercell formed by 18 layers perpendicular to the (111) fcc direction, containing 56 atoms each. The lattice constant is initially taken to be 4.05 \AA . The direction (111) corresponds to that in which the contact is elongated until breakdown. Simulations are performed at 4 K. In a first stage the system is relaxed during 50 picoseconds. After this relaxation, two bilayer slabs are defined at the top and bottom of the relaxed supercell, and are separated at a velocity of 2 m/s. The atoms inside these slabs are frozen during subsequent stages, defining the bulk supports of the nanocontact during the breaking process. The other atoms move and reaccommodate into new configurations during the elongation process. The full determination of atomic positions during contact stretching allows the evaluation of the evolution of its minimum cross-section S_m . The determination of S_m has been done by considering a standard numerical procedure, which is able to determine the nanocontact slice with the smallest cross-section S_m in number of atoms [18]. The slice

thickness is assumed to be equal to the covalent atom diameter. With this methodology, S_m can result in a non integer value when, for instance, the contact atomic layers are irregular.

Following a similar strategy to that of nanocontact transport experiments, we performed many numerical realizations of wire breakages for the statistical analysis of the conductance. For all scans, and resulting configuration each 20 ps, we computed the conductance using a full quantum mechanical procedure based on the *ab initio* Gaussian embedded-cluster method [19]. Due to computer time limitations, the conductance was computed for configurations with $S_m \leq 5$ restricting the quantum calculation to a nanocontact region formed by 5 atomic layers, describing the narrower (and most important, in terms of electronic transport) nanocontact section. This narrow layer is formed by the minimum cross section layer (where S_m is evaluated) and its two neighboring layers below and above. A similar strategy has been recently proposed [20] for constructing computational gold conductance histograms, although a parameterized Tight-Binding approach has been used to calculate conductance values.

Typical evolution of the minimum cross-section S_m , and the corresponding conductance G , during the nanocontact breakage are shown in Figure 1. The shapes of the curves reveal the existence of a strong correlation between conductance and the nanocontact neck section size, in agreement with previous numerical results for other materials [4,18,21]. A striking fact is that for values $S_m \approx 1$ (defining a nanocontact of one-atom section) there are two different conductance values ($G/G_0 \approx 2$ and ≈ 1). These values correspond to different atomic arrangements [3]. On the one hand, the monomer contact configuration (see Figure 1a) provides conductance values of the order of $G/G_0 \approx 2$, while on the other hand, the dimer contact configuration (see Figure 1b) gives rise to conductances close to $G/G_0 \approx 1$. This conductance bi-valuation, for the $S_m \approx 1$ case, shows that the orbital valence accommodates differently depending on the contact coordination and on the separation between the contact atom and its neighbors, a finding that confirms previous observations [3,22]. Also, we have noticed that when a neck section of two-atom contact lifts under stretching, a dimer-chain contact is formed, giving rise to a conductance jump from a value greater than 3 to 1.2

(see Fig. 1b). With increasing stretching (time in the figure), G slowly decreases and then increases from $0.90G_0$ to $1.05G_0$. This occurs when the dimer–chain contact evolves from a position perpendicular to the (111) direction towards a parallel alignment with this direction (which is perpendicular to the supporting slabs). Such increase of G before the rupture, reproduces STM transport measurements [23], confirming the validity of our model, and reveals the possible improvement of electronic resonant conditions with strain, as predicted by previous numerical calculations [5,23]. Finally, when the contact breaks, one reaches the tunnelling regime and the conductance falls to 0 as the nanocontact ceases to stretch.

For more than 800 aluminum nanocontact configurations (obtained from the evolution of 50 stretching sequences), we estimated the conductance per minimum cross–section $G_a = G/S_m$, which is equivalent to the sum of the three channel transmitivities available for aluminum atoms at the narrowest neck section. Figure 2 depicts G_a as a function of the minimum cross–section S_m . In spite of the data dispersion, the figure suggests that G_a converges to a constant value as S_m increases. We recall that the independence of G_a on the contact size has been previously observed experimentally for gold nanocontacts [4], where it was observed that $G_a = G_0$, which is the maximum possible value for the atomic conductance of any monovalent material [4,16,21]. For the aluminum case, Fig. 2 shows that for almost all configurations, G_a results larger than G_0 , and converges to a value between G_0 and $1.5G_0$. Then, the data suggests that aluminum nanocontacts are, per atom, better conductors than any monovalent metal wire.

As usually done in experiments [14,15,24–26], we accumulated all G traces and constructed the first computational aluminum conductance histogram (see Fig. 3, top). The good agreement between this numerical result and previously published experiments, again evidences the good fidelity of our calculations, i.e. aluminum conductance histogram peaks are close to integer multiples of the conductance quantum [24–26]. We recall that a peaked structure has been also observed in minimum cross-section histograms [13,20], reflecting the existence of energetically favorable atomic configurations at the nanocontact neck. Regarding experiments, the main advantage, when performing molecular dynamics simulations,

is that we can separate the corresponding conductance contributions in nanocontact configuration families, grouping configurations that possess a similar number of atoms at the narrowest nanocontact cross-section. In order to identify such configuration families, we use the integer label N_a ($N_a = 1, 2, 3, \dots$) to describe the set of configurations with minimum cross-section S_m comprised between $N_a - 1/2$ and $N_a + 1/2$. This label is equivalent to the effective number of atoms defining the narrowest nanocontact region. Partial conductance histograms concocted in the previous fashion are depicted in Fig. 3 and show that for all N_a values, there corresponds a peak at a conductance value $G_M(N_a)$. For comparison, we also show in Figure 3 the average conductance $\langle G(N_a) \rangle$ for each partial conductance histogram (see vertical dashed lines). Note that for the monoatomic contact case ($N_a = 1$), two conductance peaks appear at $G/G_0 = 1$ and $G/G_0 = 2$, which correspond, respectively, to the conductance contributions of the dimer-chain (see inset of Fig. 1b), and the single-central one-atom (see inset of Fig. 1a) contact configurations. For $N_a \geq 2$ the average conductance $\langle G(N_a) \rangle$ is close to the peak position $G_M(N_a)$ indicating that conductance distributions are rather symmetrical around its maximum value.

Figure 4 plots the quantity $G_M(N_a)/N_a$ (open circles) as a function of the effective number of atom contacts N_a . In this Figure, we have included two points corresponding to particular aluminum nanocontact configurations with $N_a = 20$ and 30 . The convergence of the atomic conductance to a constant value between 1 and 1.5 is now much more evident than in Figure 2. Figure 4 also includes a plot of the conductance maximum $G_M(N_a)$ as a function of N_a (gray squares, corresponding label figure appears at the right hand side). The good quality of a linear fit of the data ($\chi^2=0.9995$) suggests that the conductance converges to a straight line (with a slope of $1.16 G_0$). Additionally, we plot the average conductance $\langle G(N_a) \rangle$ for each contact configuration family N_a (small black circles in Fig. 4), and its corresponding standard error. Within the estimated error bars, the $\langle G(N_a) \rangle$ values reflect the same linear behavior observed for $G_M(N_a)$. Therefore it is evident that a linear relation between the conductance and the effective number of atom contacts N_a can be established. The slope of the curve is now an electronic structure specific property that can be bundled

into a peculiar *ballistic resistivity* defined by

$$G = N_a/\rho_b$$

where N_a is dimensionless and $1/\rho_b$ has the dimensions of conductance. Here, ρ_b retains the value of $0.86 R_0$, where R_0 denotes the quantum unit resistance, or 12907Ω .

Semiclassical approximations based on the free electron model have a fundamental shortcoming in the face of the previous result: They only depend on geometry, and the Fermi wavelength is the only material dependent parameter, while backscattering due to both geometrical and electronic structure constraints are the main culprit for the appearance of ballistic resistance in nanomaterials [2,21]. In our conductance calculations, the scattering phenomenon is implicitly described in the considered quantum methodology. In that sense the new ballistic resistivity cannot be interpreted as *ohmic*, but a result of a novel scaling behavior of the material conductance at the mesoscale. It is this scaling that promises to be a universal material independent property. In such transport regime, where the mean free path of electrons is larger than the sample size, the conductance dependence on the contact length loses meaning, while the dependence on the cross-sectional size is preserved as in many theoretical approximations (i.e the Sharvin conductance is proportional to the contact minimum cross-sectional area A). In our work, the notion of the area A , instead of N_a , is inadequate since any consideration defining it in a complex electronic structure of few atom contacts results speculative. Notwithstanding it is intuitive that a first order approximation for such an area should behave linearly with the effective number of atom contacts N_a .

Finally, one should expect that the described ballistic resistivity ρ_b will also depend on thermodynamical variables, as the the minimum cross-section histograms depend on temperature [13]. Such properties, and the extension of this kind of studies on other chemical elements with different electronic structures, seem to conform a field of a promising research activity, due to the obvious attractive applications of these knowledge in the emerging nanoelectronic industry.

REFERENCES

- [1] Landauer, R. Electrical resistance of disordered one-dimensional lattices. *Phil. Mag.* **21**, 863-867 (1970).
- [2] Scheer, E., Agraït, N., Cuevas, J.C., Levy-Yeyati, A., Ludoph, B., Martín-Rodero, A., Rubio Bollinger, G., van Ruitenbeek, J.M., & Urbina, C. The signature of chemical valence in the electrical conduction through a single-atom contact. *Nature* **394**, 154-157 (1998).
- [3] Jelinek, P., Pérez, R., Ortega, J. & Flores, F. First-principles simulations of the stretching and final breaking of Al nanowires: mechanical properties and electrical conductance. *Phys. Rev. B* **68**, 085403 (2003).
- [4] Rodrigues, V., Fuhrer, T. & Ugarte, D. Signature of atomic structure in the quantum conductance of gold nanowires. *Phys. Rev. Lett.* **85**, 4124-4127 (2000).
- [5] Lee, Y. J., Brandbyge, M., Puska, M. J., Taylor, J., Stokbro, K. & Nieminen, R. M. Electron transport through monovalent atomic wires. *Phys. Rev. B* **69**, 125409 (2004).
- [6] Cuevas, J.C., Levy Yeyati, A. & Martín-Rodero, A. Microscopic origin of conducting channels in metallic atomic-size contacts. *Phys. Rev. Lett.* **80**, 1066-1069 (1998).
- [7] Sharvin, Y.V. A possible method for studying Fermi Surfaces. *Zh. Eksp. Teor. Fiz.* **48**, 984-985 (*Sov. Phys. JEPT* **21**, 655-656 (1965)).
- [8] Torres, J. A., Pascual, J. I. & Sáenz, J. J. Theory of conduction through narrow constrictions in a three-dimensional electron gas. *Phys. Rev. B* **49**, 16581-16584 (1994).
- [9] Olesen, L., Laegsgaard, E., Stensgaard, I., Besenbacher, F., Schiøtz, J., Stoltze, P., Jacobsen, K. W. & Nørskov, J. K. Quantized conductance in an atom-sized point contact. *Phys. Rev. Lett.* **72**, 2251-2254 (1994).
- [10] Agraït, N., Rodrigo, J. G. & Vieira, S. Conductance steps and quantization in atomic-

- size contacts. *Phys. Rev. B* **47**, 12345-12348 (1993).
- [11] Krans, J. M., van Ruitenbeek, J. M., Fisun, V. V., Yanson, I. K. & de Jongh, L. J. The signature of conductance quantization in metallic point contacts. *Nature* **375**, 767-769 (1995).
- [12] Costa-Krämer, J. L., García, García-Mochales, P. & Serena, P. A. Nanowire Formation in Macroscopic Metallic Contacts: A universal Property of Metals. *Surf. Sci.* **342**, L1144-L1152 (1995); Erratum in *Surf. Sci.* **349**, L138 (1996).
- [13] Hasmy, A., Medina, E. & Serena, P.A. From favorable atomic configurations to super-shell structures: a new interpretation of conductance histograms. *Phys. Rev. Lett.* **86**, 5574-5577 (2001).
- [14] Medina, E., Díaz, M., León, N., Guerrero, C., Hasmy, A., Serena, P.A. & Costa-Krämer, J.L. Ionic shell and subshell structures in aluminum and gold nanocontacts. *Phys. Rev. Lett.* **91**, 026802 (2003).
- [15] Yanson, A.I., Yanson, I.K., & van Ruitenbeek, J.M. Observation of shell structure in sodium nanowires. *Nature* **400** 144-146 (1999).
- [16] Yanson, A.I., Yanson, I.K., & van Ruitenbeek, J.M. Crossover from electronic to atomic shell structure in alkali metal nanowires. *Phys. Rev. Lett.* **87** 216805 (2001).
- [17] Mishin, Y., Farkas, D., Mehl, M. J. & Papaconstantopoulos, D. A. Interatomic potentials for monoatomic metals from experimental data and ab initio calculations. *Phys. Rev. B* **59**, 3393-3413 (1999).
- [18] Bratkovsky, A. M., Sutton, A. P. & Todorov, T. N. Conditions for conductance quantization in realistic models of atomic-scale metallic contacts. *Phys. Rev. B* **52**, 5036-5051 (1995).
- [19] Palacios, J. J., Pérez-Jiménez, A. J., Louis, E., SanFabián, E. & Vergés, J. A. First-

- principles approach to electrical transport in atomic-scale nanostructures. *Phys. Rev. B* **66**, 035322 (2002).
- [20] Dreher, M., Heurich, J., Cuevas, J. C., Scheer, E., & Nielaba, P. Theoretical analysis of the conductance histograms of Au atomic contacts. *arXiv:con-mat/0406281 v1* (11-jun-2004).
- [21] Nakamura, A., Brandbyge, M., Hansen, L.B. & Jacobsen, K.W. Density Functional Simulation of a Breaking Nanowire. *Phys. Rev. Lett.* **82**, 1538-1541(1999).
- [22] Lang, N. D. Resistance of atomic wires. *Phys. Rev. B* **52**, 5335-5342 (1995).
- [23] Cuevas, J. C., Levy Yeyati, A., Martín-Rodero, A., Rubio Bollinger, G., Untiedt, C. & Agraït, N. Evolution of conducting channels in metallic atomic contacts under elastic deformation. *Phys. Rev. Lett.* **81**, 2990-2993 (1998).
- [24] Yanson, A. I., & van Ruitenbeek, J. M. Do histograms constitute a proof of conductance quantization? *Phys. Rev. Lett.* **79** 2157-2157 (1997).
- [25] Díaz, M., Costa-Kramer, J.L., Serena, P.A., Medina, E. & Hasmy, A. Simulations and experiments of aluminum conductance histograms. *Nanotechnology* **12**, 118-120 (2001).
- [26] Halbritter, A., Csonka, Sz., Kolesnychenko, O. Yu., Mihály, G., Shklyarevskii, O. I., van Kempen, H. Connective neck evolution and conductance steps in hot point contacts *Phys. Rev. B* **65**, 045413 (2002).

Acknowledgments. We thank J. J. Sáenz for helpful discussions, and Cecalcula (Venezuela) for computer facilities. This work has been partially supported by the CSIC-IVIC researchers exchange program and the Spanish DGICYT (MEC) through Projects MAT2000-0033-P4 and BFM2003-01167/FISI.

Correspondence and requests for materials should be addressed to A.H. (e-mail: anwar@ivic.ve).

FIGURES

FIG. 1. Figures (a) and (b) illustrate two examples of the time evolution of the minimum cross-section (black symbols) and the quantum conductance (open symbols) during aluminum wire breakages. The results are obtained from a combination of Embedded Atom Molecular Dynamics and ab-initio Gaussian Embedded-cluster method, respectively. The temperature is equal to 4K. The insets show some of the atomic configurations at the contact region. (a) illustrates a rupture mechanism which passes through a single-central atomic configuration before breakage. (b) illustrates the formation of a dimer-chain contact before breakage. Arrows and dashed vertical lines denote the corresponding conductance and minimum cross-section associated to these nanoneck configurations. Note that the dimer-chain and the single-central atom contact have a similar minimum cross section value ($S_m \approx 1$), but the conductance results equal to G_0 and $2G_0$, respectively. The stretching mechanism in (b) involves a rotation of a dimer unit at the nanoneck. For larger necks, the results suggest that there is a proportionality factor between the minimum cross-section and the conductance.

FIG. 2. The conductance per minimum cross-section G_a (i.e. the quantum conductance divided by the minimum cross-section) plotted as a function of the minimum cross-section for all configurations, results from fifty simulated aluminum nanocontact breakages. In spite of the data dispersion, it is observed that such atomic conductance is larger than G_0 and converges to a constant value as the contact size increases. The dotted line is a guide to the eye, which denotes the quantum conductance value.

FIG. 3. The top of the figure shows the calculated conductance histogram for aluminum. It includes more than 800 nanocontact configurations. The peak structure of the histogram is reminiscent of what has been previously observed in aluminum conductance experiments. Below this histogram, we separately show the contribution to the global conductance histogram of configurations corresponding to effective number of atoms $N_a = 1, 2, 3, 4, 5$ and 10. Such number of atoms is equivalent to the calculated minimum cross-section value, but in integer precision. We observe that in each histogram there appears a maximum at a conductance value $G_M(N_a)$ (bins corresponding to these maxima were filled with gray). Vertical dashed lines show the computed average conductances $\langle G(N_a) \rangle$ for each depicted conductance distribution.

FIG. 4. The conductance per atom is plotted as a function of the effective number of atom contacts N_a (open circles). Here, the convergence to a constant atomic conductance value is more evident than in Fig. 2. The figure label at the right hand side refers to the conductance $G_M(N_a)$ curve (gray symbols) for the respective number of contact atoms. A linear fit gives a slope equal to 1.16, suggesting that this is the value for which the atomic conductance should converge for larger nanocontact sizes. The figure also shows the corresponding average conductance $\langle G(N_a) \rangle$ for each value of the effective number of atom contacts (black circles, the bars indicate the respective standard error of the conductance mean), and shows that this estimation is also consistent with the linear fit. The results demonstrate the proportionality between conductance and number of atoms N_a , and reveals the existence of a transport parameter which does not depend on the contact size. The inverse value of the slope (0.86) denotes an effective ballistic resistivity of preferable atomic configurations for aluminum nanocontacts.

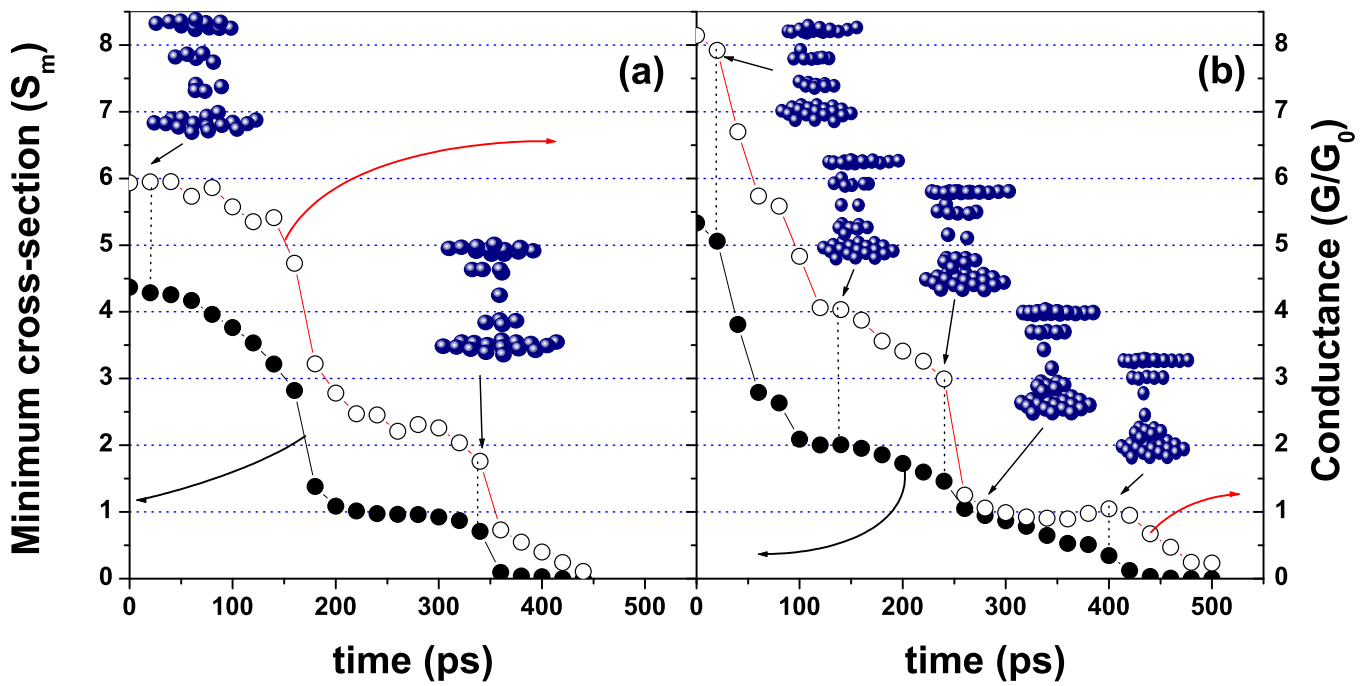


Figure 1

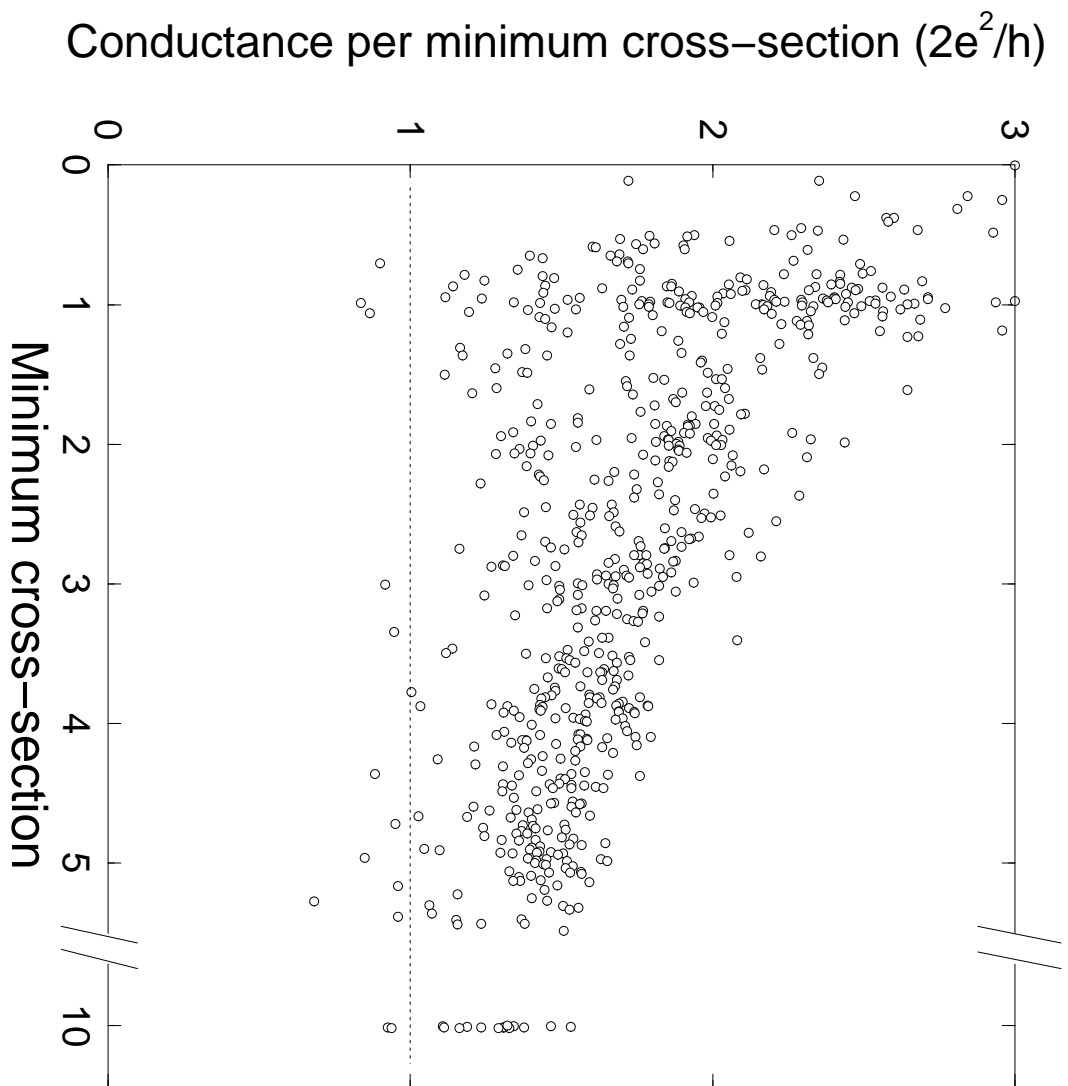


Fig. 2

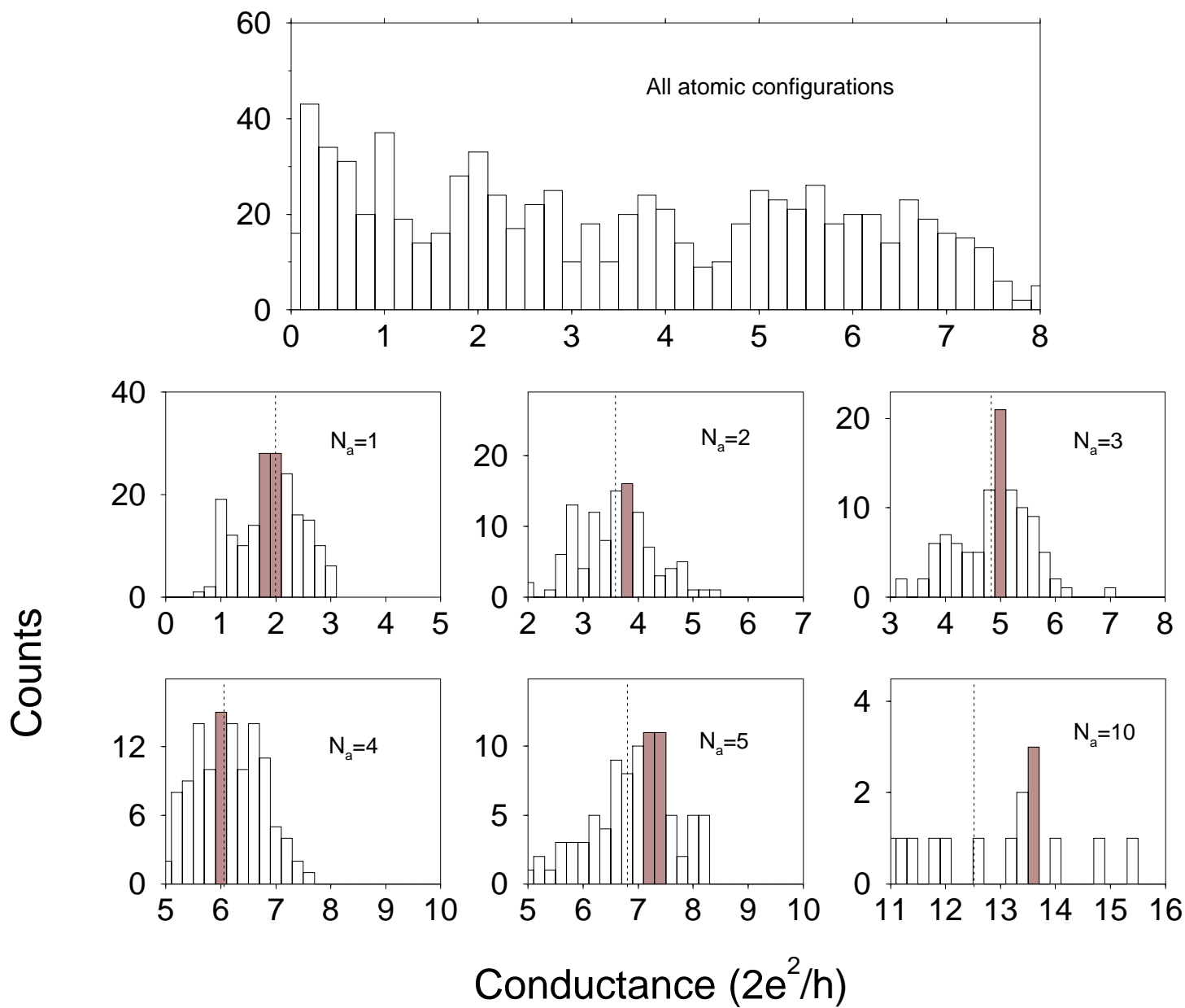


FIG. 3

Fig. 4

